

CHIRAL SYMMETRY BREAKING MODELS FOR PRE-BIOTIC ENVIRONMENTS

[Awards Symposium, ACS, New Orleans, April 9, 2013]

ABSTRACT:

Molecular biology of living organisms depends fundamentally on chiral preferences (*e.g.*, L vs. D amino acids). Historically, several theoretical scenarios have been proposed to explain how this stereochemical bias might have spontaneously arisen from a non-chiral, or at least racemic, environment. In addition, some key experiments have been described in the scientific literature which generically exhibit these kinds of chiral symmetry breaking and amplification. This lecture will present two distinct theoretical models with the same objective, to describe spontaneous chiral symmetry breaking in terms of detailed molecular level processes. One model starts with only non-chiral reactants and involves only reversible physical and chemical rate constants; the other incorporates irreversible stirring disturbance in a racemic slurry, generating crystal fracture and leading to Ostwald ripening phenomena. Both models produce spontaneous symmetry breaking over widely variable time scales, depending upon the choice of kinetic rate inputs.

=====

[View 1.](#) Title, Princeton collaborators, funding

=====

The preferential handedness (chirality) of terrestrial biomolecules is pervasive, and the chemical and physical processes that are basic to life utilize that chiral preference to great structural advantage. Without chiral enantiomer dominance, biochemistry would be stalled to the point of complete inactivity with an overwhelming preponderance of structurally useless molecules. In other words, chiral enantiomer dominance is evidently a necessary condition for life as we conventionally define it. That leads to the natural question about how chiral bias might have arisen in order to allow life to originate here on the Earth, if not elsewhere in the Universe. Not surprisingly considerable theoretical and experimental effort has been devoted to identify such physical-chemical scenarios in what presumably was an essentially racemic (unbiased) initial state of our planet. This brief lecture will outline two contrasting theoretical models, each consistent with their own corresponding experiments. Understanding them may help to clarify what actually happened here (and perhaps elsewhere) billions of years ago as a first stage of planet-wide chiral symmetry breaking. It should be stressed at the outset that these models describe individual molecular-level processes, as opposed to macroscopic (mass action) descriptions of overall kinetics. Time limitation means that this presentation of two aspects of a very complex subject will necessarily be rudimentary and incomplete.

As obligatory background, the next View 2 shows schematic representations of the

=====
[View 2.](#) D (R) and L (S) forms of alanine
=====

two mirror image forms of the simple amino acid molecule alanine. As with 18 other proteinogenic amino acids (non-chiral glycine is the single exception) it is the L form that appears almost exclusively in living organisms, at least on the Earth. Similar stereochemical distinctions exist for building blocks of other biomolecules such as sugars. The extremely rare exceptions of D amino acids incorporated in biomolecules appear to be post-transcription modifications imposed for special biological purposes. Although the D, L labeling is conventionally used for amino acids in molecular biology, a different geometric labeling convention for chiral molecules, using R and S, is more widely accepted in stereochemistry.

Out of the very large scientific literature already devoted to this problem of chiral symmetry breaking, the next View 3 lists some papers that are relevant for the first of the

=====
[View 3.](#) Some relevant papers: background, recent detailed description
=====

two theoretical models to be presented here. The 1953 publication by F.C. Frank is widely recognized as an historical landmark for the field. The last paper listed is our recently published, very detailed, description of this first model. It is designed to describe qualitatively the overall physical chemistry of spontaneous chiral symmetry breaking in a uniform liquid medium. For ease of visualization, computation, and presentation, it has been developed theoretically with reactants and products residing on a two-dimensional square lattice. This amounts to a molecular level configurational coarse-graining that retains focus on the central phenomena of interest. Such extreme simplifications are not an intrinsic necessity however. The model can readily be elevated to three dimensions (*e.g.*, residing on a cubic lattice), or even to "real" three-dimensional continuum space. However those modifications do not qualitatively change the kinetic behaviors that can be illustrated already in the simple and graphic two-dimensional version.

A liquid solution of two non-chiral reactant species constitutes the chemical starting point. These are small reactant molecules A that occupy one lattice site, and larger reactant molecules B₂ that occupy a nearest-neighbor pair of sites. Multiple occupancy of lattice sites is forbidden. View 4 presents a specific example of a one-third-filled square

=====
[View 4.](#) Two-dimensional lattice model, 12×12, 16 A's, 16 B₂'s, achiral configuration
=====

lattice with equal numbers of the two reactant species. The visually "empty" sites should be regarded as occupied by inert solvent molecules that play no explicit role in subsequent chemical kinetics. The configuration shown is an example of many possible

A+B₂ configurations on the lattice obviously possessing no intrinsic left-handed *vs.* right-handed preference. It has reflection symmetries (both horizontal and vertical), which guarantee that it is intrinsically free from two-dimensional chiral bias. Such an unbiased arrangement of reactants and solvent can serve (and often has served) as a starting point for numerical studies of the evolution over time of this model. One postulates that this system is in contact with a thermal reservoir to maintain a chosen temperature *T*. The resulting thermal agitation causes the reactants to undergo nearest-neighbor translational and rotational diffusive jumps on the lattice, to come into nearest-neighbor contact, and to undergo reversible chemical reactions.

Three distinct reversible interaction processes are present. The first of these is illustrated in View 5, whereby an A+B₂ reactant pair diffuse together into one of two

=====

[View 5.](#) Isolated A+B₂ diffuse together, form a bent contact, and react, with reversals; both R and S product molecules are illustrated, distinguished by red *vs.* blue. Covalent chemical bonds are indicated by heavy line segments.

=====

distinguishable bent nearest-neighbor contact arrangements, then undergo a reversible chemical reaction creating a chemical bond to form a correspondingly bent left or right handed (R or S) product molecule AB₂ ($\equiv C_{R/S}$). With one important exception the forward and reverse rates for this reaction are independent of the occupancy of the immediately surrounding neighbor sites. These forward and reverse reaction rates are formally represented by simple Boltzmann factors containing respectively positive activation energies E_f and E_r multiplied by $\mathbf{b} = 1/k_B T$; this elementary form is utilized primarily as a book-keeping simplification.

The important exception mentioned is illustrated in the following View 6.

=====

[View 6.](#) Autocatalysis geometry

=====

It constitutes a positive feedback mechanism to encourage symmetry breaking by involving autocatalysis. If an A, B₂ reactant pair find themselves by diffusion in a bent configuration within the cleft of an already-formed product molecule C_{R/S} of the same bent chirality, an enhanced Boltzmann factor reaction rate and a correspondingly enhanced reverse rate exist with reduced activation energies $0 < E_f^{cat} < E_f$ and

$$0 < E_r^{cat} < E_r.$$

One other feedback mechanism is also postulated, involving heteroinhibition. In this case it is a negative feedback process. It is illustrated in View 7. This involves two

=====

[View 7.](#) Heteroinhibition

=====

chemically bonded $AB_2 = C_{R/S}$ products that are chiral opposites and that have diffused together so as to occupy one another's clefts simultaneously. They can then "react" (*i.e.*, undergo minor readjustments relative to one another on the occupied lattice sites) to form a non-covalently bound state, with binding energy $e > 0$, indicated in the View 7 by dotted lines, due to dispersion-attraction and possibly intermolecular hydrogen bonding. This is another reversible process, but because no covalent chemical bond formation is involved, no activation energy has been introduced for formation of this heteroinhibition cluster, nor for its breakup which has only the requirement of "going uphill" by binding energy amount e . Notice that because this cleft-filling heteroinhibition deactivates equal numbers of R and S product molecules, if some chiral asymmetry were already present it would disproportionately lower the fraction of minor enantiomers that remain available for autocatalytic formation of their own kind.

For our investigations a Monte Carlo numerical procedure acts as a thermal reservoir with a chosen temperature, and thanks to its embedded random number generator it stochastically drives the time-dependent evolution of this model system, starting with a suitable initial condition. One such initial condition was illustrated in the prior View 4, in which only reactants and inert solvent molecules were present in a geometric pattern that is intrinsically unbiased toward either left or right handedness. Because the magnitudes of the various forward and reverse rates are under the investigator's control it is possible to disentangle their separate influences on the kinetic outcome of an ensemble of Monte Carlo runs.

Indeed as proposed by F.C. Frank 60 years ago, autocatalysis and heteroinhibition can be an effective kinetic combination for spontaneous chiral symmetry breaking. The Monte Carlo investigations carried out on this first model support that position, at least over a significant time span. However the present model goes beyond the F.C. Frank macroscopic analysis by providing a detailed molecular-level description of the many-body system evolution as time progresses.

As is no doubt well known, a direct measure of chiral symmetry breaking is "ee", the enantiomeric excess. For completeness it is defined in View 8. Note that while $ee=0$

=====

[View 8.](#) Definition of "ee"

=====

refers to a racemic mixture of equal numbers of R and S molecules, it could also be extended to include cases in which no chiral molecules of either R or S handedness have yet been formed. Numerical simulations for the model normally involve carrying out a significant number of Monte Carlo runs to determine time (t) dependence of the model's state, with identical initial and process-rate (temperature, transition-state energy) choices. In particular this produces a distribution of ee(t) results. Statistically reproducible symmetry breaking of an achiral starting configuration amounts to appearance and at least temporary persistence of a bimodal ee distribution for such an ensemble of Monte Carlo runs.

The following View 9 shows the time dependence for two sets of 40 Monte Carlo runs

=====

[View 9.](#) [Fig. 4] (a) $E_f/E_r=1$, (b) $E_f/E_r=0.5$; for both cases $e/E_f = 0$, $bE_f = 10$,

$E_f^{cat}/E_f = 0$; N_C is the total number of product molecules $C_{R/S}$; no heteroinhibition is involved; one-third-filled 36×36 lattice.

=====

on a one-third-filled 36×36 lattice (with periodic boundary conditions), where equal numbers (144) of initial A and B₂ reactants were present in an initial configuration containing no chiral bias. At any given time, N_C denotes the total number of chiral product molecules present. For these runs there is no heteroinhibition underway. The two contrasting cases displayed illustrate the profound effect that reaction reversibility can have. In case (a) the rapid reverse reaction undoing AB₂ chiral product molecules very quickly turns an early-stage non-zero "ee" transient for each run into a statistical racemic situation. But when the activation energy for the reverse reaction is doubled while other parameters remain unchanged, (b), there suddenly appear long-lived non-zero ee's. But note that these individual run ee's are broadly distributed, not displaying the bimodal ee distribution expected for valid chiral symmetry breaking. It should be mentioned that larger system sizes (60×60) have also been used with the same coverage fraction 1/3, with no perceptible system size effect. The time unit t appearing in these plots represents the average time between successive Monte Carlo visits to any one of the particles present, whether those visits involve stochastic choice of transition (diffusion, reaction) or no change, with relative probabilities determined by the chosen rates.

View 10 shows what happens to the ee distribution when a sudden temperature boost

=====

[View 10.](#) [Fig. 5] $bE_f(\text{initial}) = 10$, $bE_f(\text{final}) = 5$. All simulations had

$E_f/E_r = 0.5$, $e/E_f = 0$, $E_f^{cat}/E_f = 0$, $j = 1/3$, 36×36 lattice, no heteroinhibition.

=====

by a factor of 2 is applied at the end of a set of runs of the preceding kind 9(b). The long-time-persisting chiral biases present before the sudden heating, quickly relax toward racemic systems, then exhibit only statistical fluctuations about zero.

The following View 11 illustrates the powerful effect that adding heteroinhibition to

=====

[View 11.](#) [Fig. 6] (a) $e/E_f = 0$, (b) $e/E_f = 10$. All simulations had $bE_f = 12$,

$E_f/E_r = 0.9$, $E_f^{cat}/E_f = 0$, $j = 1/3$, 36×36 lattice.

=====

case 11(a), creating case 11(b), can produce, while other parameters remain unchanged. Once again 40 runs were generated on 36×36 lattices at 1/3 coverage with periodic boundary conditions for both versions. Notice the factor of 10 increase in time scale from plot 11(a) to plot 11(b), the former showing sigmoidal racemizations, the latter

showing distinctive bimodal appearance of a long-time persistence of symmetry breaking.

The next View 12 shows results for a 40-run ensemble where both feedback

=====
[View 12](#). [Fig. 7] (a) Overall ee(t) values for 40 simulations; (b) monomer-only $|ee_{adj}(t)|$ for AB_2 products; (c) typical trajectory showing $100\times|ee_{adj}(t)|$ in red, $N_A(t) = N_{B_2}(t)$ in green, $N_C(\text{monomer})$ in blue, $N_{\text{het.dimer}}(t)$ in black. All simulations have $bE_f = 12$, $E_f / E_r = 0.88$, $E_f^{cat} / E_f = 0.35$, $e / E_f = 10$, $j = 1/3$, 36×36 lattice.

=====
mechanisms were operating. Thus there is strong mutual inhibition and strong autocatalysis. But there is also appreciable reverse reaction rate. As with all previous examples shown the initial configuration was intrinsically free from chiral bias. Perhaps the most important feature of these last results is how nearly enantiopure the solution of unbound (undimerized) product molecules becomes and persists, measured by an adjusted ee, $|ee_{adj}|$. This amounts over an ensemble of many repetitions to a persistent vividly bimodal ee distribution for C monomers, that is, the effectiveness of a "monomer purification" mechanism. Of course the number of unbound product molecules is declining slowly over time as the system approaches ultimate racemization.

The time scale of kinetic processes being studied is strongly dependent on the initial concentration of reactants. This has been the reason for predominately using $1/3$ lattice coverage. Going to much lower coverage (dilute solution) might be more "realistic", but it stretches out the Monte Carlo simulations to an impractical extent due to the much longer time for reactants to diffuse about before finding one another to react, or for pairs of mirror-image product molecules to find each other for heterodimer formation. In any case, our exploratory results created with modest coverage reductions below $j = 1/3$ do not suggest any qualitative change in the chiral symmetry breaking scenario, including the relative effects of the individual rate processes, just an expanded time scale.

The striking phenomenon of monomer purification that occurs in the presence of strong heterodimer binding, even when substantial rates of C decomposition (reverse rate) are present, indicates that this behavior would also arise in a three-dimensional, more physically realistic, scenario. This encourages one to formulate estimates in real-time units of how long the monomer enantiopurity stage could persist in three dimensions. Once the monomer purification stage has been established, the numerical simulations show that the reactant concentrations $[A](t) = [B_2](t)$ accurately obey second-order kinetics as they form C molecules of the minor chirality, then to be sequestered in heterodimers. Recall that these temporary reactants appear from dissociation of C product molecules, essentially all of the same chirality, that are not bound in heterodimers. This simplification opens the way to identify the circumstances under

which the mechanism could lead to monomer ee persistence times with possible geological relevance.

The following View 13 offers a specific example of such time-scale relevance.

=====
[View 13.](#) Rough estimate of system parameters producing geological-time-scale $|ee_{adj}|$ persistence. System size (1 meter)³; concentration of reactant A at beginning of racemization stage is 10^{-5} mol/l; typical bimolecular reaction rate for $T \approx 300K$; racemization time $\approx 10^6$ yr; 1 meter diffusion time for serine in water ≈ 5 yr.

=====
It assumes that the initial reactant concentrations at the beginning of the monomer-purified stage have a reasonable low concentration for a biological metabolite, and a typical value is assigned for the bimolecular kinetic rate at $T \approx 300K$. The implied half life for decay to the overall racemic state is then found to be $\approx 10^6$ yr. This far exceeds the estimated time for diffusion over an assumed (1 meter)³ system size, using the measured diffusion constant for serine in water as a relevant example, namely ≈ 5 yr. Therefore this first model can in principle maintain chiral symmetry breaking over geological times. Of course different choices of the model's basic rate parameters can increase the characteristic persistence times by further orders of magnitude.

The second theoretical model is built upon a variant of the "Ostwald ripening" phenomenon. The basic features of that phenomenon are presented in View 14. This

=====
[View 14.](#) Ostwald ripening

=====
simple version involves the temporal evolution of the crystal size distribution in undisturbed liquid-suspended crystal slurries as molecules enter the liquid from crystals, diffuse, and rejoin crystals, causing slow kinetic convergence onto a single large crystal. The kinetic driving force is that small crystals have higher solubility than larger crystals of the same substance, causing the latter to grow at the expense of the former. Compared to the amount of substance contained in the crystals, the amount dissolved in the liquid might be relatively small if the solvent is limited in amount, or is not a very good solvent for the substance involved. In any case the liquid solution would be close to saturation. The Ostwald ripening process applies in general both to non-chiral and to chiral substances and their crystals. It is important to note that as the crystal size distribution moves toward larger average size, the rate of change of that size distribution tends to slow down very markedly, so that the theoretically expected final emergence of a single large crystal might take an extremely long time.

Unlike the previous liquid phase model, the second chiral-symmetry-breaking scenario to be described does not include covalent bond formation or molecular dissociation processes. Instead it starts with a given, possibly racemic, mixture of R and

S stereoisomers of a single molecular substance. These molecules remain fixed in total R + S number over time, and will be distributed between a liquid solvent phase and coexisting enantiopure R and S crystals. This model exists in three dimensions, dispenses with a lattice, allows single molecules in the liquid solution to convert spontaneously between R and S forms, and follows their passage between the liquid and crystal phases. As results to be shown will make clear, the numbers of molecules to be considered in numerical simulations for this second case far exceed the range that was numerically feasible in the prior lattice model simulations.

Developing this second model was motivated by experiments showing that vigorous stirring with glass beads, causing grinding of racemic (or nearly racemic) slurries containing those enantiopure R and S crystals, eventually led to development of overall enantiopurity for the crystalline portion of the system within a reasonable time span. This type of scenario involving an application of Ostwald ripening to chiral crystals is usually called "Viedma ripening". A few of the many relevant papers for this class of processes are listed in the next View 15.

=====

[View 15.](#) Some relevant publications, second model

=====

The primary objective of our second model is to document the time dependence of enantiomeric excess in systems of those R and S chiral variants, whether just for the crystals, for just the liquid solution, or indeed for the entire system. The intention is to provide a situation in which an Ostwald-Viedma ripening process now acting simultaneously on two kinds of crystals (enantiopure R and S) can be significantly accelerated by externally applied mechanical interference to keep the crystals small, thus retaining the early-stage speed of Ostwald ripening. In fact under proper circumstances the result is attainment of substantially identical chirality for all crystals in a considerably shortened time span, and that overall enantiopurity for the collection of crystals remains while the stirring and grinding continue. This last feature qualitatively distinguishes this model's behavior from that of the first model, which inevitably relaxes toward racemization in the long-time limit.

The basic features of this attrition-enhanced Ostwald ripening model are identified in View 16. These include four distinct rate processes underlying the time-dependent

=====

[View 16.](#) Basic features of the attrition-enhanced Ostwald ripening model

=====

distribution of R and S species within the liquid solution and among the individually enantiopure crystals forming the agitated slurry. Two of the four rate processes are reversible: liquid-phase racemization, and crystal size change by dissolution or growth through monomer exchange with the solution. The other two rate processes are irreversible, stemming from the mechanical agitation due to vigorous stirring. These

latter two are single-crystal attrition (fracturing) into a random-size-separated pair of smaller crystals due to grinding, and crystal agglomeration as stirring brings pairs of crystals of the same chirality $i = R, S$ into forced contact with proper orientation to bond, thus creating a larger crystal. For simplicity this last process is assumed most likely to occur by addition of dimers (number of molecules $m = 2$) to possibly larger crystals ($m' \geq 2$). Both of these irreversible processes would be absent if the externally supplied stirring process were suddenly to cease. As was the case with the previous model, the system is in thermal contact with a fixed-temperature heat bath, but now that heat bath must act to absorb the heat constantly generated by the mechanical energy of stirring.

It should be noted in passing that this second model is still under active investigation. The details presented in the last View 16 may not be precisely those included in a final publication. However we do not expect any qualitative changes in the primary features displayed thus far by the model.

Although the crystal attrition (fracturing) acts to enhance the rate of Ostwald ripening, it also places the small fragments produced at risk of quickly dissolving and then losing chiral memory by liquid phase racemization. This is at least partially neutralized by the agglomeration process. Dimers and their intrinsic chirality become rescued by inclusion in the larger enantiopure crystals of the same chirality that are less at risk of totally dissolving.

Without engaging in undue speculation, one might consider how a system of the sort postulated by this second model could possibly experience vigorous stirring in a real planetary environment. Certainly convection due to thermal gradients, gases bubbling up through a slurry, or even ambient wind currents would be possibilities. More energetic disturbance conceivably could arise from geyser-like conditions or even effects from geological plate tectonics.

In this second model, although the total number of enantiomers $N_R(t) + N_S(t)$ is constant over elapsed time, any enantiomer molecule can switch chirality at the pre-assigned rate when in the liquid phase. While in a crystal the molecules cannot invert, but they can redissolve and then be subject to inversion. There will be some number $n_R^{(m)}(t)$ and $n_S^{(m)}(t)$ of crystals composed of $m \geq 2$ enantiomers of type R or S present at time t . Formally $m = 1$ will refer to dissolved monomers. As was the case in the preceding model, this second case specifies and monitors configurational details at the molecular level.

Numerical simulations for this model, as for the prior one, utilize the Monte Carlo method to implement the various transitions at the appropriate relative rates. In order to follow the chiral symmetry breaking processes, it is of course necessary to monitor the entire inventory of R and S molecules as a function of elapsed time. The subsequent View 17 provides details of the time-dependent chiral molecule inventory, from that of

=====

[View 17](#). Chiral molecule inventory

=====

the chosen initial condition ($t=0$) to later stages of symmetry breaking and amplification. Note that primary interest concerns enantiopurity of the crystal phase; the liquid solution always contains both R and S molecules, but would be removed (decanted) at the final stage of a real experiment.

View 18 illustrates the kind of initial condition used for the Monte Carlo simulations

=====
[View 18.](#) Initial crystal size distributions prior to stirring/grinding disturbance

=====
of this second model, namely Gaussian distributions of crystal size, assumed to lie in the range $2 \leq m \leq 100$ for both enantiomer-pure R and S crystals. The example shown involves a slight non-zero ee, but in other circumstances equal R and S crystal distributions have also been used for racemic initial conditions. The "noise" appearing in these distributions arises from the necessity of rounding the Gaussian functions to the nearest integer. A small percentage of the molecules are also assigned initially as monomers to the liquid phase, with racemic composition, for the purpose of defining liquid-phase saturation.

The considerable number of rate parameters contained in this attrition-enhanced Ostwald-Viedma ripening model leads to a substantial diversity of independent simulations that can be produced, illustrating the relative effects of parameter variations. Because of limited time, only three types of results will be considered. The next View 19

=====
[View 19.](#) (1/11/2013, page 4): $bE_{rac} = 5, p_{attr} = 0.4, K = 1, ee_0^C = 0, N = 47084,$

$$N^{eq} = N_o^L = 1000, \text{ with agglomeration [100 runs]}$$

=====
displays a set of 100 Monte Carlo simulations for the crystal slurry $ee^C(t)$ vs. number of Monte Carlo steps. All of these were started with identical initial conditions, namely $ee^C(0)=0$ and R/S saturated liquid. These runs all tend toward crystal enantiopurity as t increases, but it may be surprising how widely distributed the rates of approach to those limits are found to be.

The following View 20 presents three aspects of the chronological evolution for an

=====
[View 20.](#)

$$bE_{rac} = 5, p_{attr} = 0.4, K = 1, ee_0^C = 0.055, N_{total} = 206600, N^{eq} = 10000, N_o^L = 10000.$$

(a) ee^C , (b) $N_{R/S}^C$, (c) ee^L .

=====
ensemble of 100 systems, with a small initial bias to simplify graphics. Agglomeration is present. The View 20(c) results might seem paradoxical, because they show that the

liquid solution ee temporarily trends in the opposite direction compared to that of the crystal slurry, until enantiopurity has been obtained, followed by expected racemic character. This temporary ee^L reversal has been observed in experiments on slurry grinding (*e.g.*, Noorduin, *et al.*, 2010). In this second model it arises from agglomeration, preferentially "rescuing" dominant-chirality small crystals from dissolution, leaving minority-chirality small crystals at greater jeopardy.

The next View 21 displays the effect of varying the grinding intensity parameter p_{attr}

=====

[View 21.](#) Varying p_{attr} , other parameters the same as in View 20

=====

while holding the other parameters equal to those in the preceding set of results (View 20). Once again 100 runs were created. Finally, View 22 plots the average

=====

[View 22.](#) Average time for a run to achieve crystal enantiopurity; varying p_{attr} , other parameters the same as in View 20 and View 21

=====

deracemization time for this last set of results in View 21 as a function of p_{attr} , indicating that a shallow minimum is present identifying an optimum stirring/grinding rate.

In summary, an important distinction between the two models outlined here concerns the persistence of chiral symmetry breaking. In the first case with chemical processes occurring just in a liquid solution, reversibility of all rates inevitably implies ultimate (long-time) relaxation into a racemic state. However if the "monomer purification" mechanism of the first model is operating the system presents a very persistent, nearly complete, enantiopurity for C product monomers until overall racemization takes over. In the second case, molecules are locked into an enantiopure set of crystals for as long as the stirring/grinding operation continues. Even after turning off that stirring/grinding operation racemization need not follow because the enantiopure crystals can be immediately separated, perhaps for redissolving in some other solvent that does not host R/S transitions. However it is not presently clear how or whether this distinction between the two models is relevant to pre-biotic conditions that ultimately led to appearance of life on our own planet.

This area of research still presents many prominent scientific challenges. Are there scenarios distinctly different from those thus far considered that might have created the terrestrial pre-biotic chiral symmetry breaking? How does any one of these initial basic symmetry broken states become involved in the intrinsically coupled chemistry of the many diverse molecules that are necessary to create living and reproducing organisms? Geologists will need to clarify (if possible) the details of the early Earth's state so that relative probabilities can be assigned to the theoretically available set of symmetry

breaking scenarios. In a broader context, astrobiologists may determine if any scenarios that are historically unlikely on the Earth, due to very different physical and chemical circumstances, might underlie appearance of exotic life elsewhere in our Universe. Significant new insights into any of these open problems will certainly be welcome.

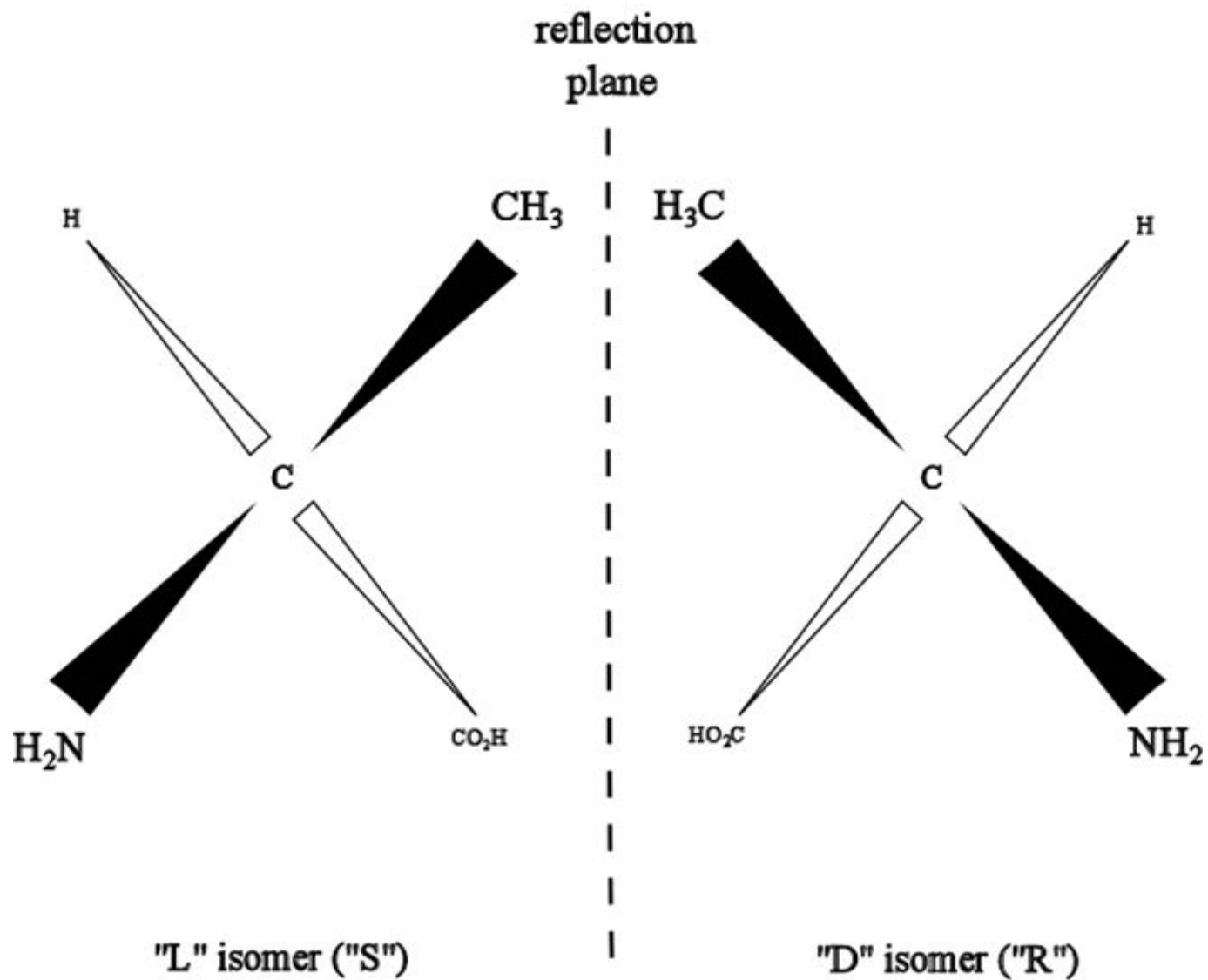
CHIRAL SYMMETRY BREAKING MODELS FOR PRE-BIOTIC ENVIRONMENTS

Pablo G. Debenedetti, Harold W. Hatch, Francesco Ricci
Department of Chemical and Biological Engineering,
Princeton University

Frank H. Stillinger
Department of Chemistry,
Princeton University

Financial support:
NSF Collaborative Research in Chemistry
(Grant No. CHE-0908265)

AMINO ACID EXAMPLE: ALANINE

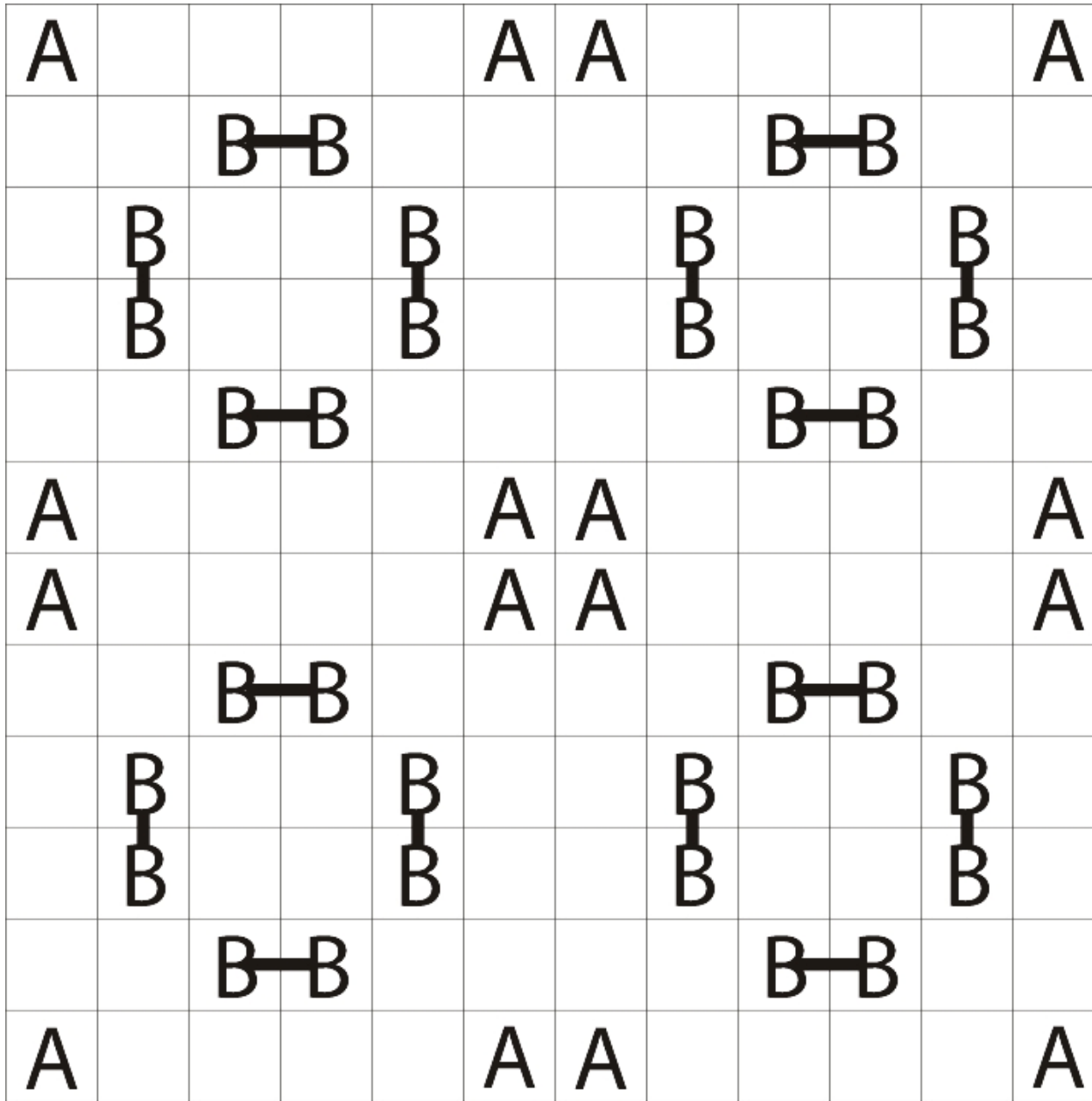


Biologically Favored

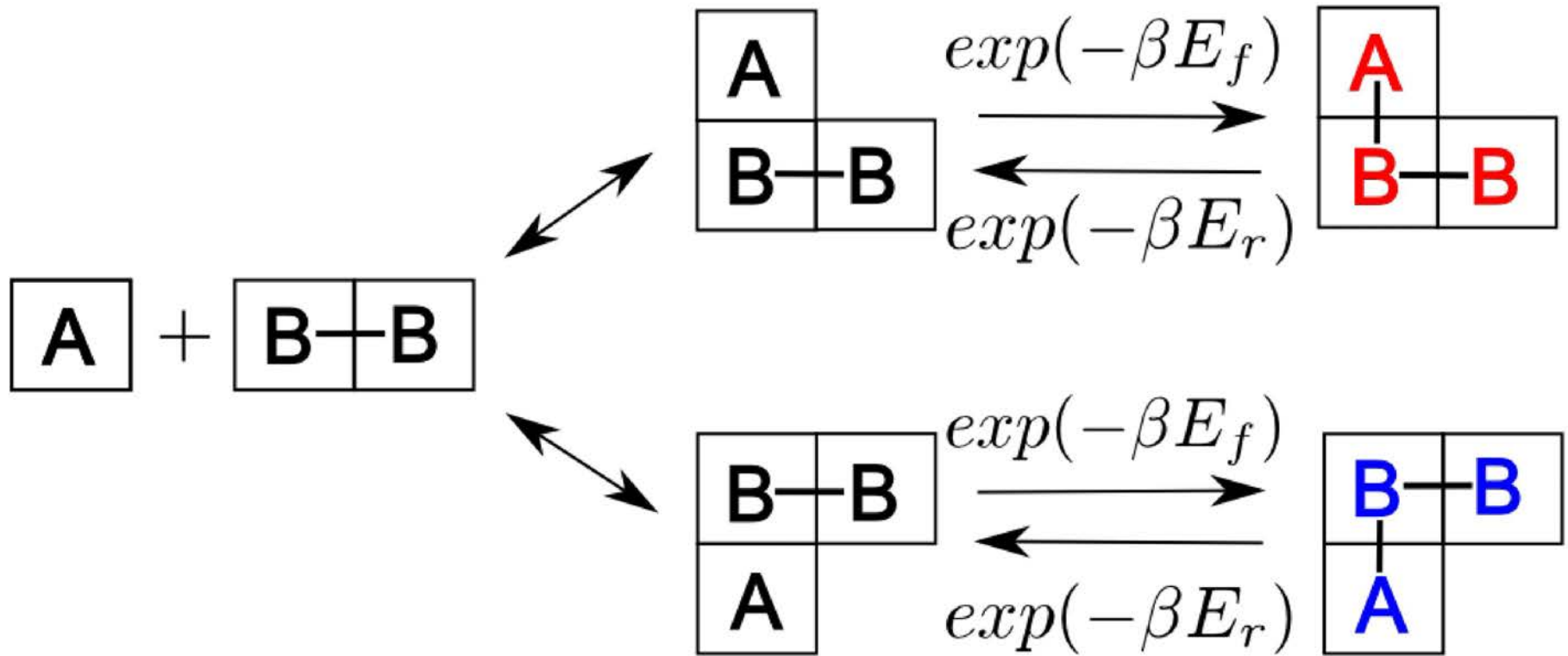
SOME RELEVANT PUBLICATIONS:
Homogeneous Solution Lattice Model
[E = experiment, T = theory]

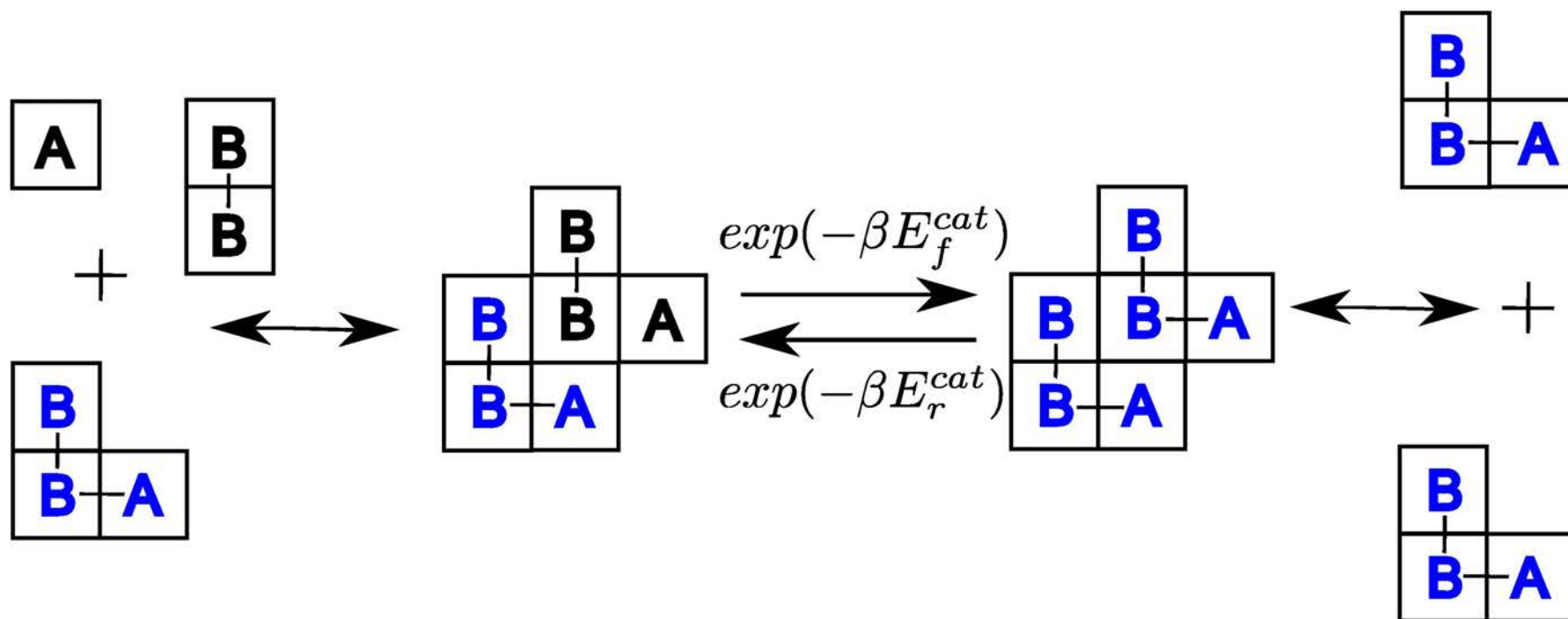
1. F.C. Frank, "On Spontaneous Asymmetric Synthesis", *Biochim. Biophys. Acta*, **11**, 459-463 (1953). [T]
2. K. Soai, T. Shibata, H. Morioka, and K. Choji, "Asymmetric Autocatalysis and Amplification of Enantiomeric Excess of a Chiral Molecule", *Nature* **378**, 767-768 (1995). [E]
3. D. Blackmond, C.R. McMillan, S. Ramdeehul, A. Schorm, and J.M. Brown, "Origin of Asymmetric Amplification in Autocatalytic Alkylzinc Additions", *J. Am. Chem. Soc.* **123**, 10103-10104 (2001). [E]
4. H.W. Hatch, F.H. Stillinger, and P.G. Debenedetti, "Chiral Symmetry Breaking in a Microscopic Model with Asymmetric Autocatalysis and Inhibition", *J. Chem. Phys.* **133**, 224502 (2010). [T]
5. F. Ricci, F.H. Stillinger, and P.G. Debenedetti, "Creation and Persistence of Chiral Asymmetry in a Microscopically Reversible Molecular Model", *J. Phys. Chem. B* **117**, 602-614 (2013). [T]

ACS
Presentation
4-9-13
F.H.
Stillinger
View 4

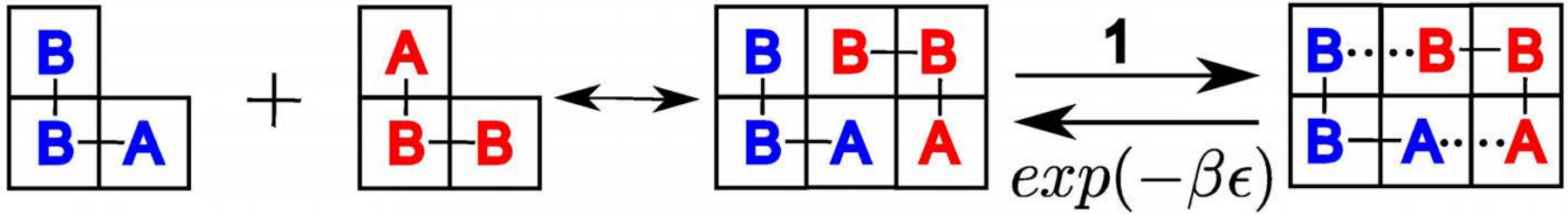


ACS Presentation 4-9-13
F.H. Stillinger
View 5



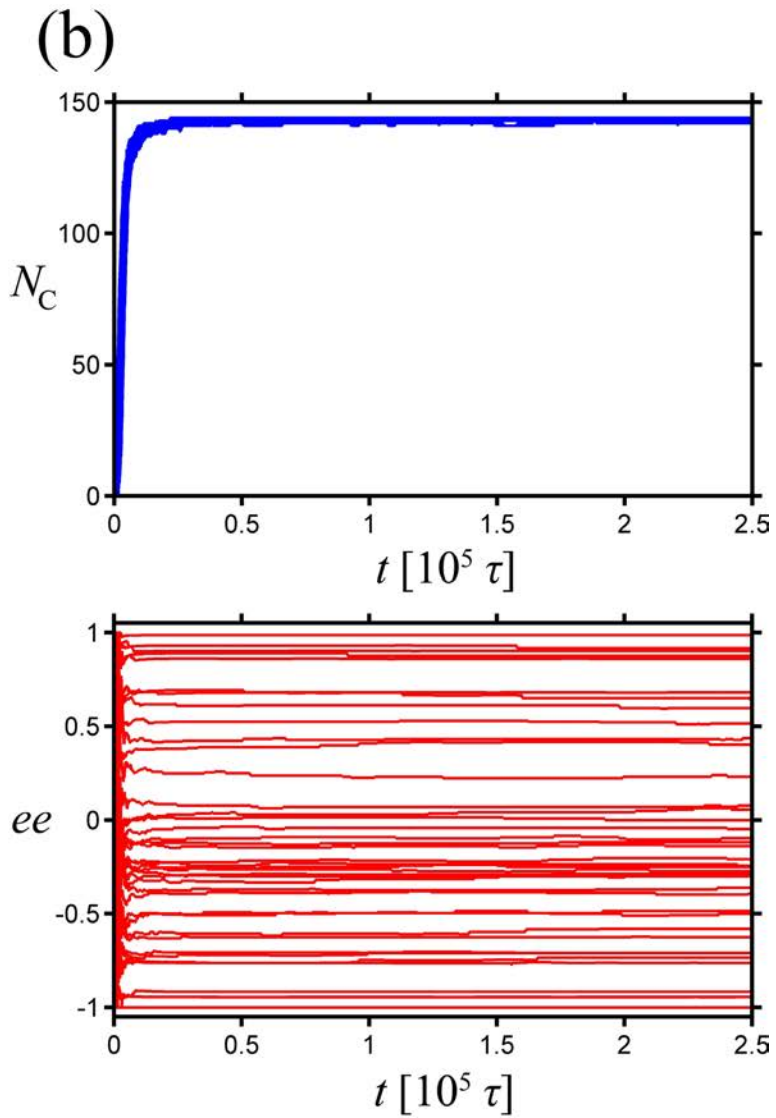
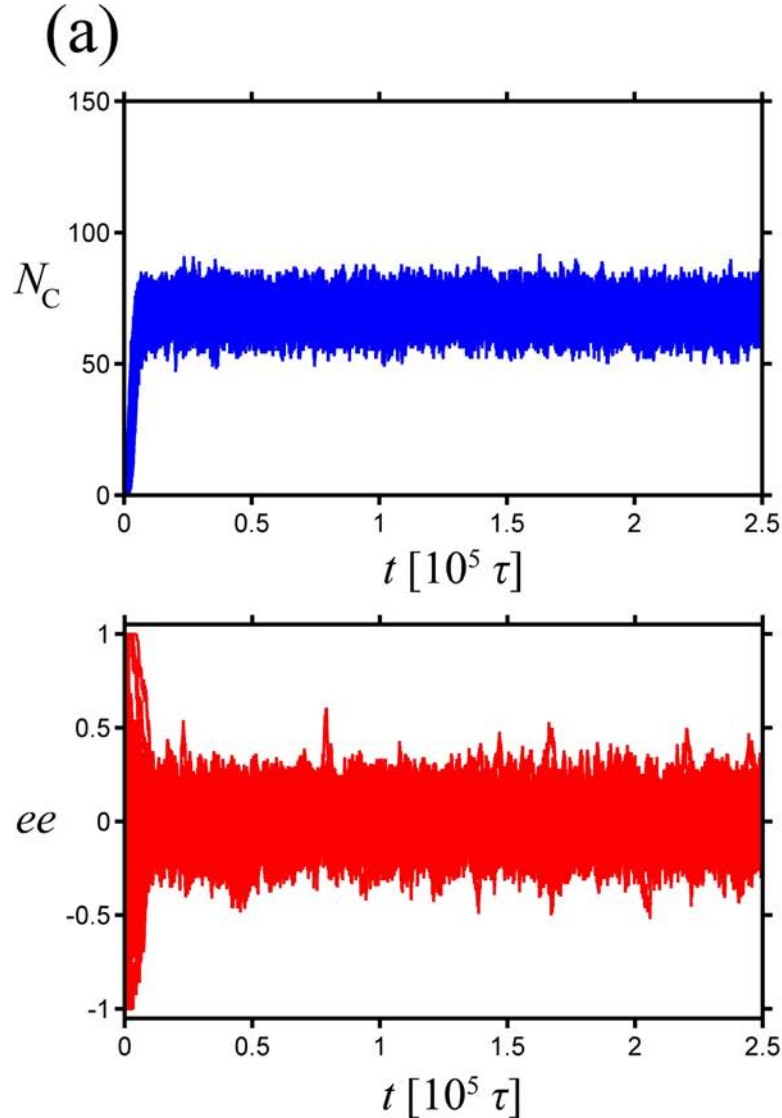


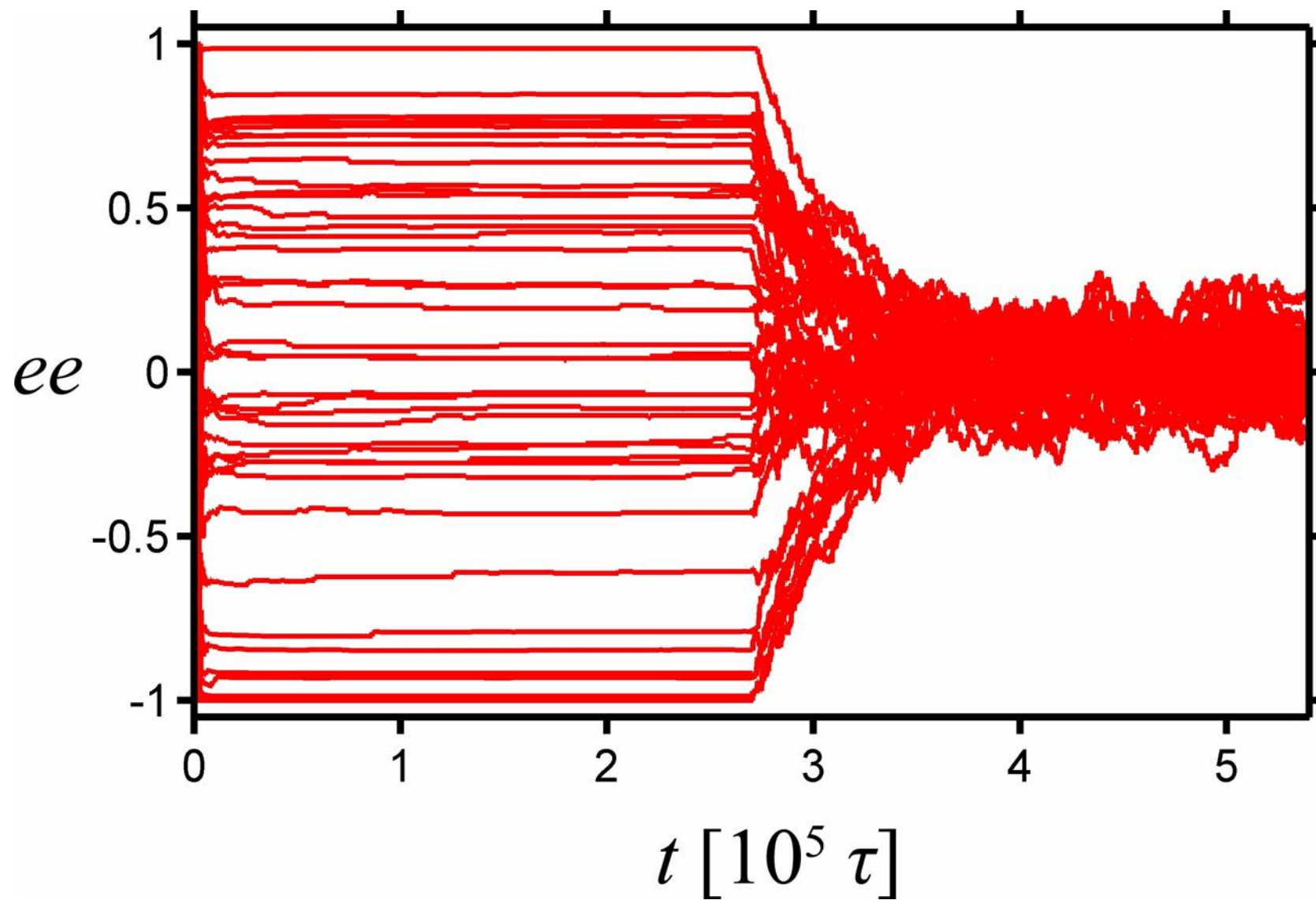
ACS Presentation 4-9-13
 F.H. Stillinger
 View 7



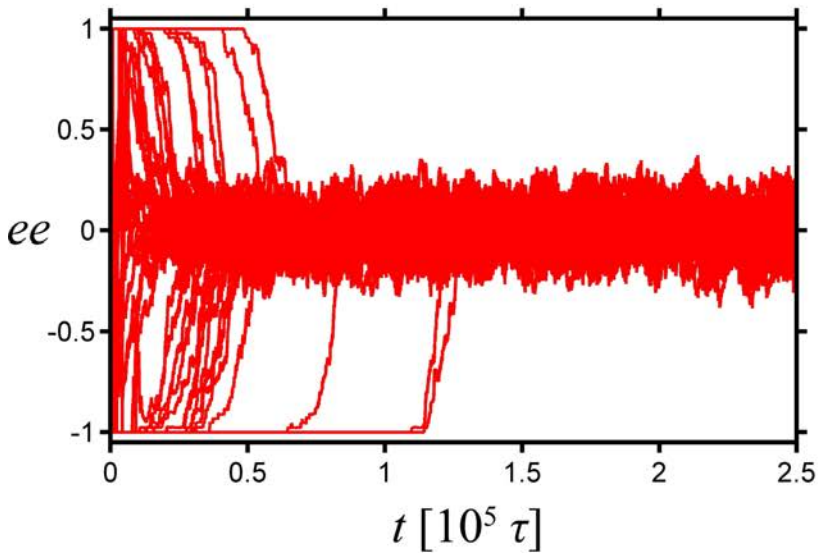
ENANTIOMERIC EXCESS "ee"

- Number of enantiomers present at time t : $N_R(t)$, $N_S(t)$
- Definition:
$$ee(t) = \frac{N_R(t) - N_S(t)}{N_R(t) + N_S(t)}$$
- Obvious limits: $-1 \leq ee(t) \leq +1$
- Racemic system: $ee = 0$
- Scalemic system: $|ee| > 0$
- Enantiopure system: $|ee| = 1$
- Indicator of chiral symmetry breaking for an ensemble of macroscopically equivalent systems is bimodality of the ee probability distribution $Q(ee)$.

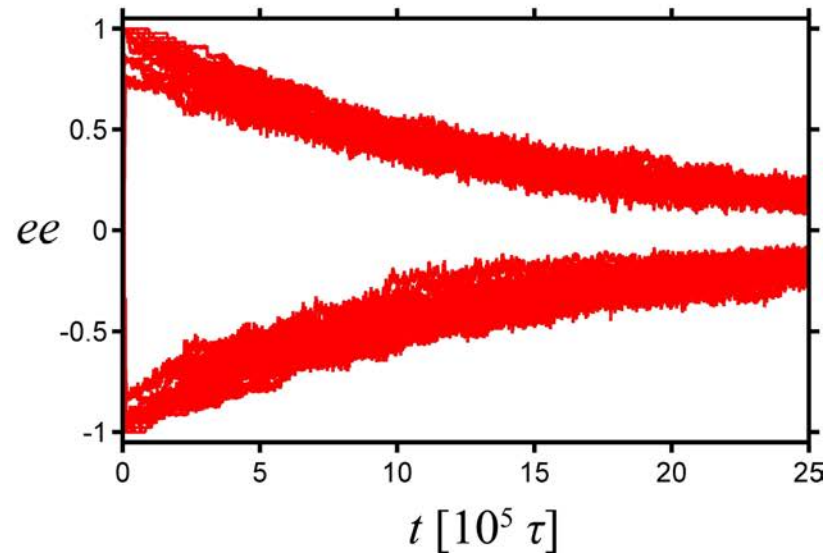




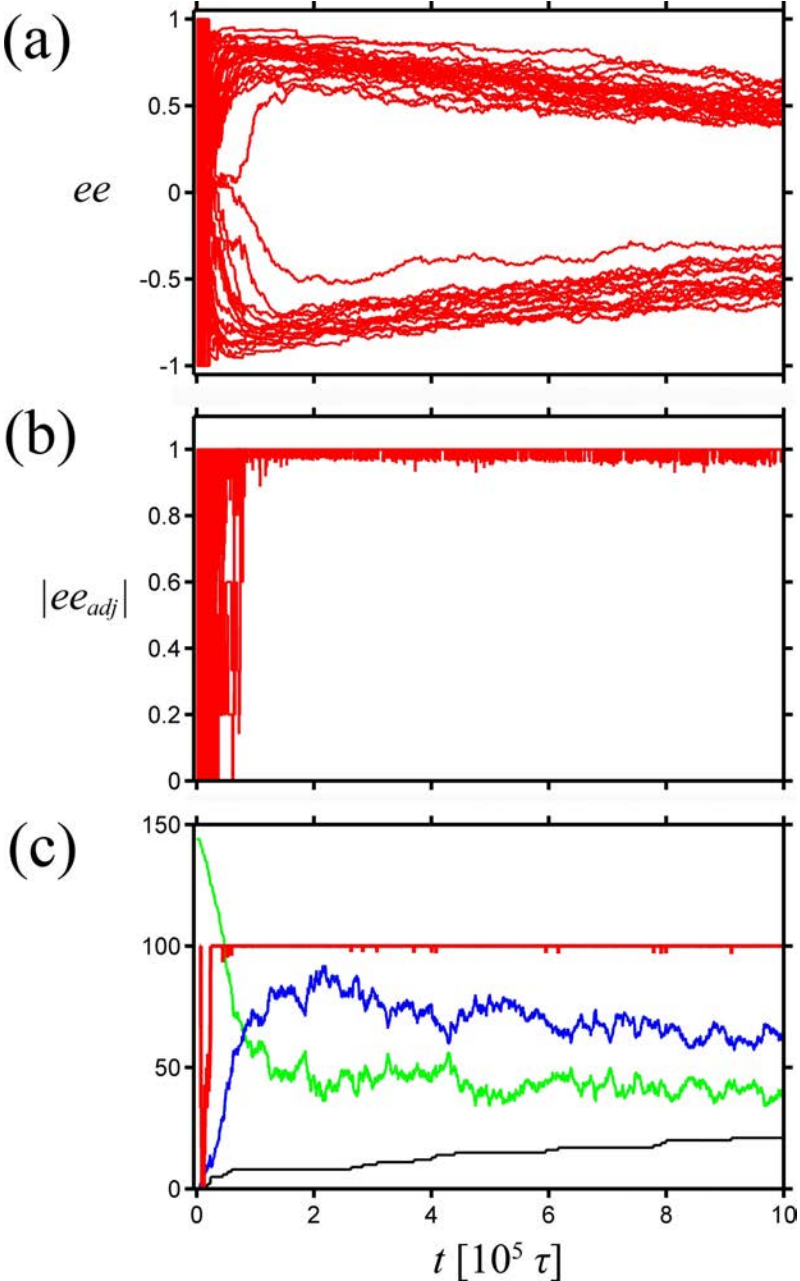
(a)



(b)



ACS Presentation 4-9-13
F.H. Stillinger
View 12



PARAMETER ESTIMATES TO PRODUCE GEOLOGICAL TIME SCALE EE PERSISTENCE

- System size $V = (1 \text{ meter})^3$; ambient T and p
- Initial reactant concentration at beginning of monomer purification stage: $[A] = [B_2] = 10^{-5} \text{ M}$
- Reverse reactions form free reactants, these combine without catalysis to form minor enantiomers, which then are sequestered in long-lived heterodimers.
- Racemization is effectively controlled by binary kinetics:

$$(d/dt)[A] = -k[A]^2$$

- Choose a representative second order rate constant:

$$k = 4.83 \times 10^{-36} \text{ m}^3 / \text{s}$$

- Implied half life of chiral persistence:

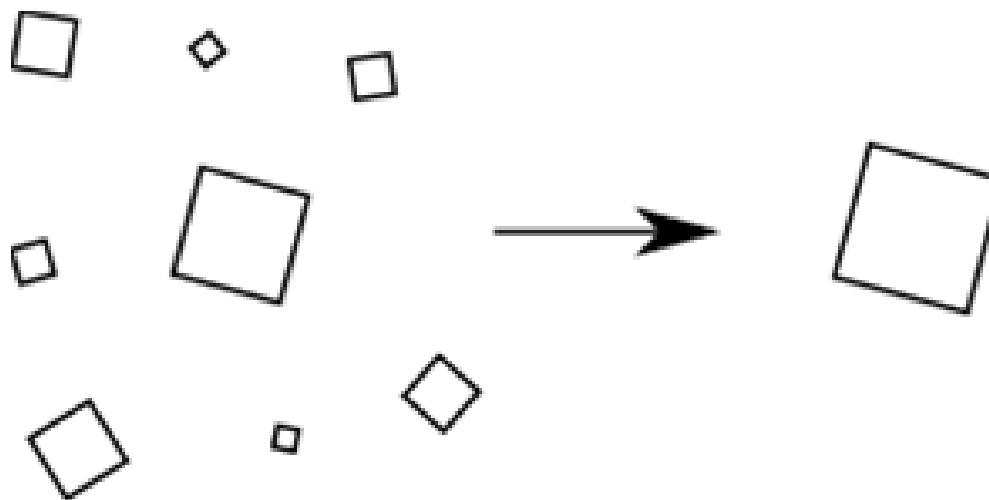
$$t_{1/2} = 1/(k[A]_{\text{in}}) \approx 10^6 \text{ yr}$$

- 1 meter diffusion time, serine in water: $\approx 5 \text{ yr}$

OSTWALD RIPENING PHENOMENON (W. Ostwald, 1896)

BACK

- Standard application refers to a size distribution of crystals composed of a single species. These are suspended in a solvent that is close to saturation in that species.
- Due to higher surface/volume ratio, smaller crystals are more soluble than larger crystals.
- Molecules preferentially leave small crystals, diffuse through the solvent, and add to larger crystals.
- Eventually only a single large crystal will remain, in contact with a solution whose near-saturation concentration is determined by that crystal's size.



SOME RELEVANT PUBLICATIONS:
Model for Three-Phase Slurry with Stirring
[E = experiment, T = theory]

1. C. Viedma, "Chiral Symmetry Breaking During Crystallization: Complete Chiral Purity Induced by Nonlinear Autocatalysis and Recycling", *Phys. Rev. Letters* **94**, 065504 (2005). [E]
2. W.L. Noorduin, H. Meekes, A.A.C. Bode, W.J.P. van Enkevort, B. Kaptein, R.M. Kellogg, and E. Vlieg, "Explanation for the Emergence of a Single Chiral Solid State during Attrition-Enhanced Ostwald Ripening: Survival of the Fittest", *Cryst. Growth Des.* **8**, 1675-1681 (2008). [T]
3. W.L. Noorduin, W.J.P. van Enkevort, H. Meekes, B. Kaptein, R.M. Kellogg, J.C. Tully, J.M. McBride, and E. Vlieg, "The Driving Mechanism Behind Attrition-Enhanced Deracemization", *Angew. Chemie* **122**, 8613-8616 (2010). [E,T]
4. J.E. Hein, B.H. Cao, C. Viedma, R.M. Kellogg, and D.G. Blackmond, "Pasteur's Tweezers Revisited: On the Mechanism of Attrition-Enhanced Deracemization and Resolution of Chiral Conglomerate Solids", *J. Am. Chem. Soc.* **134**, 12629-12636 (2012). [E]
5. H. Katsuno and M. Uwaha, "Appearance of a Homochiral State of Crystals Induced by Random Fluctuation in Grinding", *Phys. Rev. E* **86**, 051608 (2012). [T]

STIRRED THREE-PHASE SLURRY MODEL:
 CHIRAL SYMMETRY BREAKING DUE TO ATTRITION-ENHANCED
 OSTWALD RIPENING

- Fixed total number N of R and S enantiomers:

$$N = N_R(t) + N_S(t)$$

- Enantiomers present as monomers in liquid solution, and as enantiopure crystals containing $2 \leq m_i \leq N$ molecules ($i = R, S$).
- Solvent property: Monomer numbers chosen for saturated liquid
- Reversible rate processes:

- (1) Liquid phase racemization of R and S monomers:

$$p_{rac} = \exp(-\beta E_{rac}) .$$

- (2) Crystal growth or dissolution (gain/loss of monomer from/to solution):

$$\langle d / dt \rangle m_i = \alpha [\sigma_i (m_i)^{2/3} - K (m_i)^{-1/3}]$$

$$\equiv p_g ,$$

$\sigma_i =$ supersaturation ratio for $i = R$ or S .

- Irreversible rate processes, stirring-rate-determined:

- (3) Crystal attrition (random binary fracture for $m \geq 4$) by input of mechanical energy : p_{attr} .

- (4) Crystal agglomeration (dimer addition, $\Delta m = 2$):

$$p_{agglom} = p_g X_i^{(2)} , \quad X_i^{(2)} = \text{dimer fraction of } i \text{ crystals.}$$

CHIRAL MOLECULE INVENTORY

- Fixed total inventory: $N = N_R(t) + N_S(t)$,

$$N_R(t) = \sum_{m \geq 1} m n_R^{(m)}(t), \quad N_S(t) = \sum_{m \geq 1} m n_S^{(m)}(t) .$$

- At time $t \geq 0$ the liquid solution contains $n_R^{(1)}(t)$ monomers of type R , and $n_S^{(1)}(t)$ monomers of type S :

$$ee^L(t) = [n_R^{(1)}(t) - n_S^{(1)}(t)] / [n_R^{(1)}(t) + n_S^{(1)}(t)] .$$

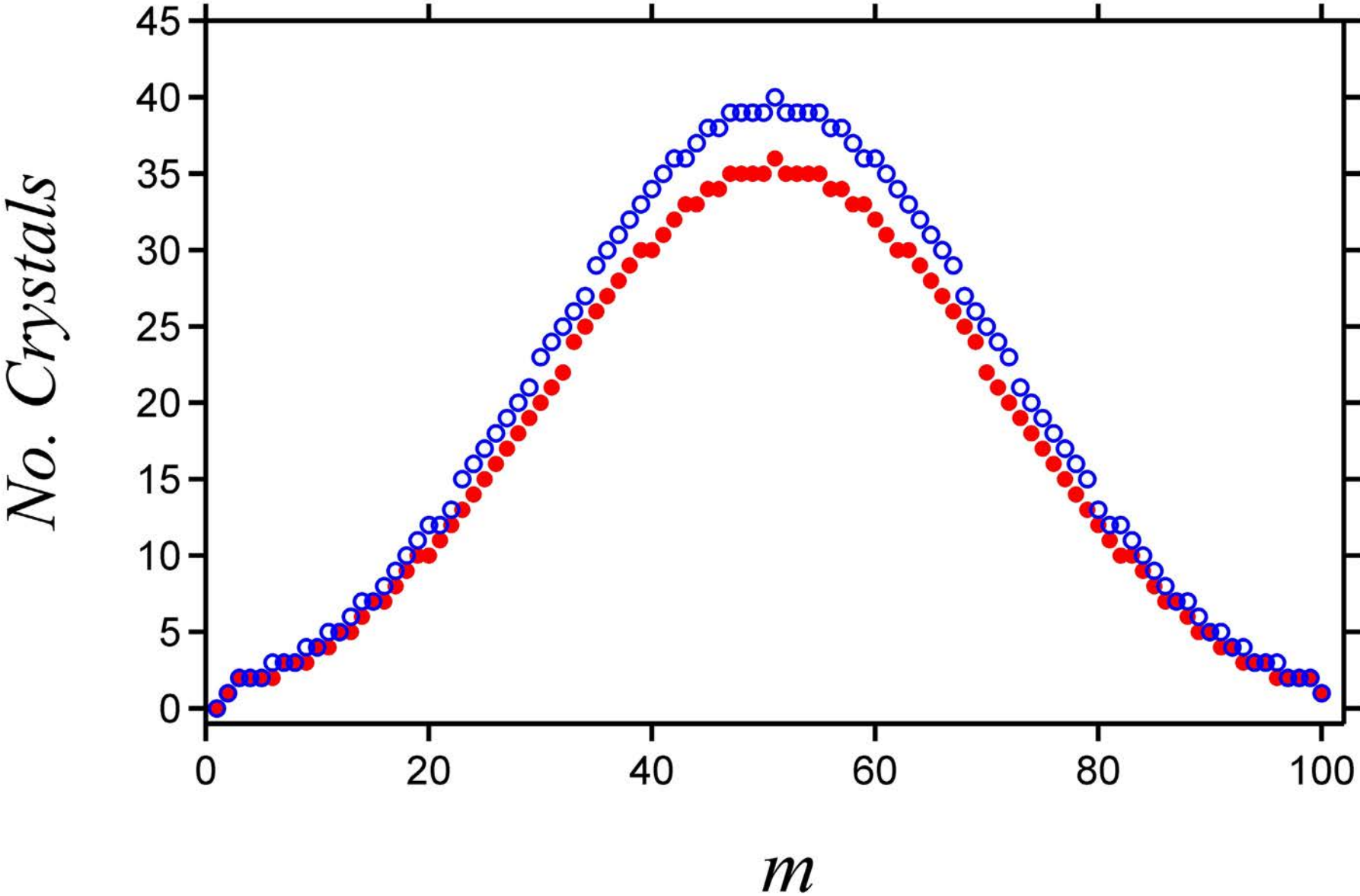
- The crystal slurry at time $t \geq 0$ consists of $n_R^{(m)}(t)$ and $n_S^{(m)}(t)$ enantiopure crystals containing $m \geq 2$ R or S molecules, respectively:

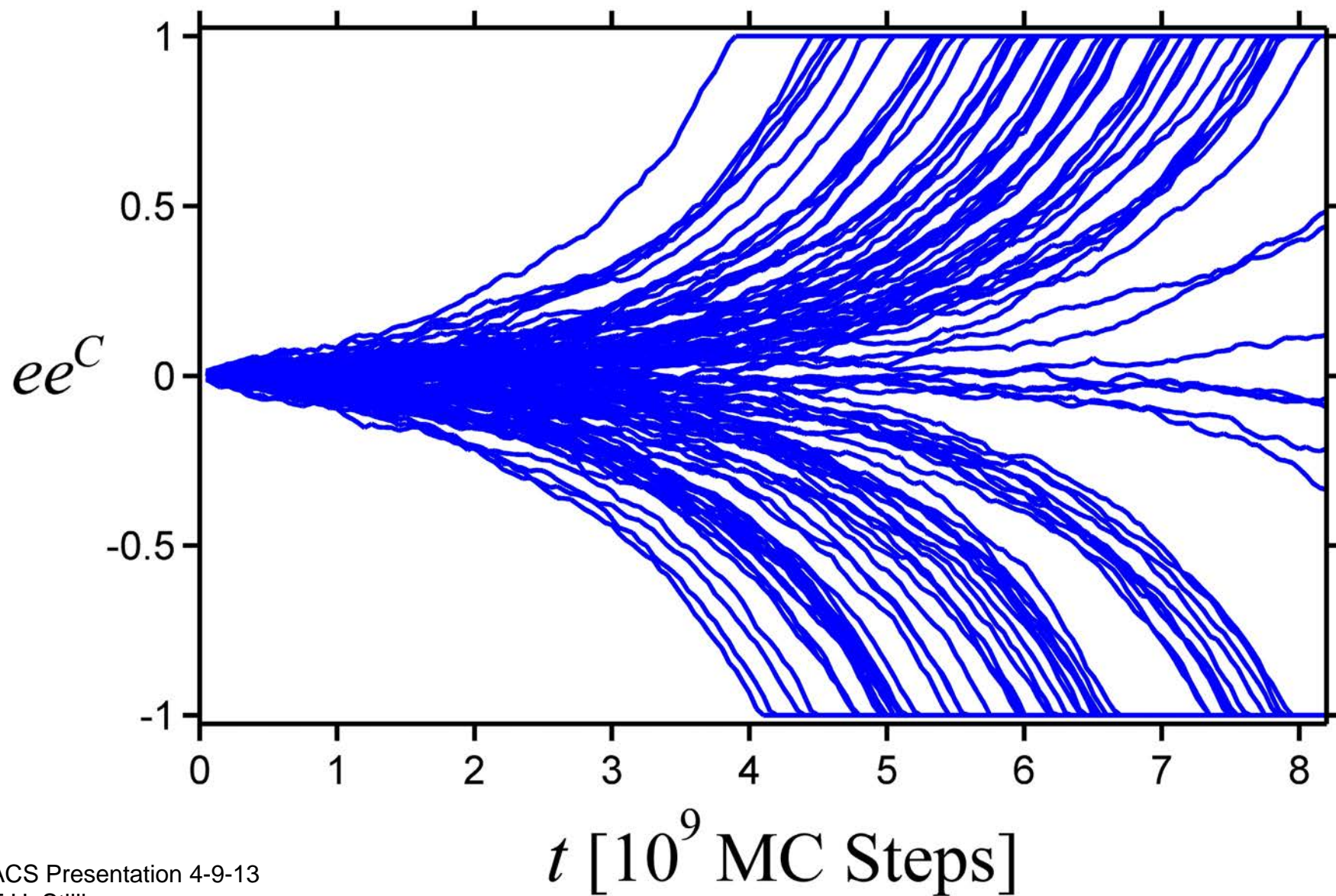
$$ee^C(t) = \sum_{m \geq 2} m [n_R^{(m)}(t) - n_S^{(m)}(t)] / \sum_{m \geq 2} m [n_R^{(m)}(t) + n_S^{(m)}(t)]$$

- Initial conditions: R and S saturated liquid with $ee^L(0) = 0$,
 $ee^C(0) \approx 0$ (racemic or slightly biased);
 Gaussian distributions of R and S crystals
 wrt. $m \geq 2$.

- Typical range of total number of molecules used in Monte Carlo simulations:

$$40,000 \leq N \leq 200,000$$

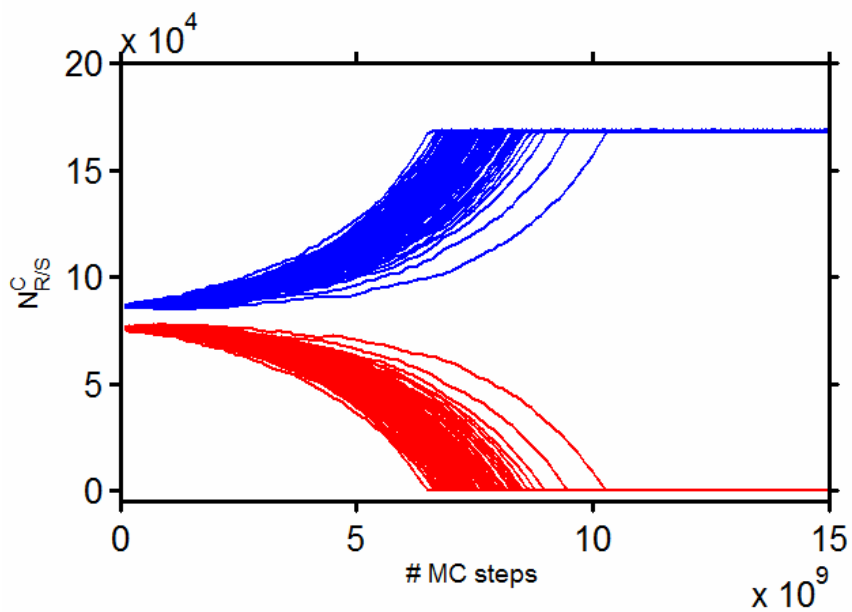
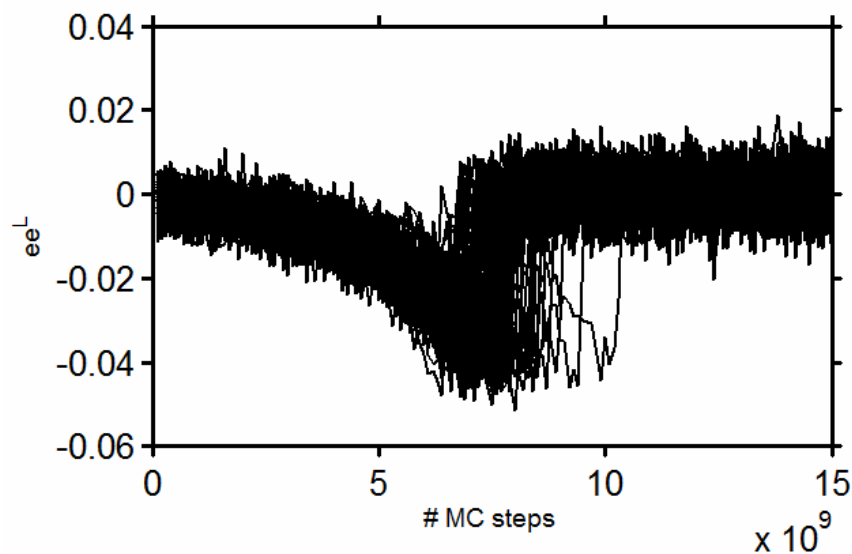
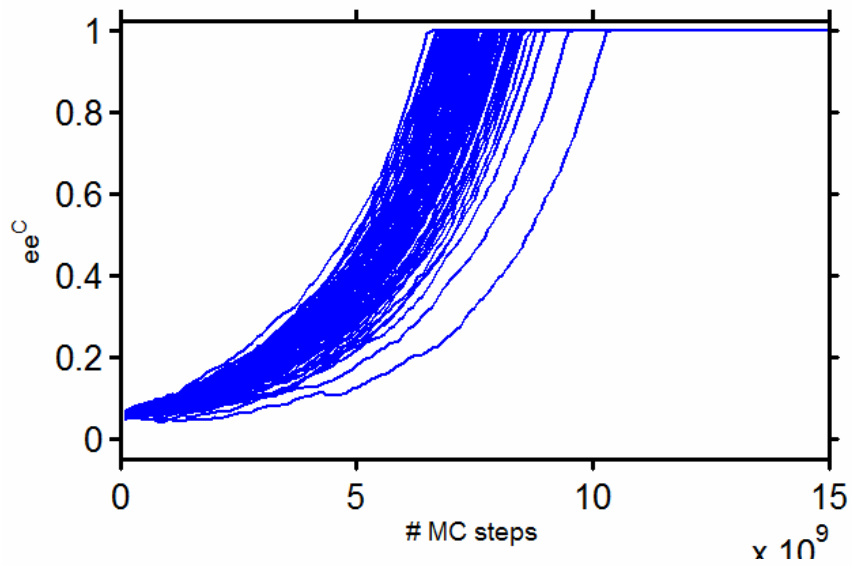




With agglomeration

BACK

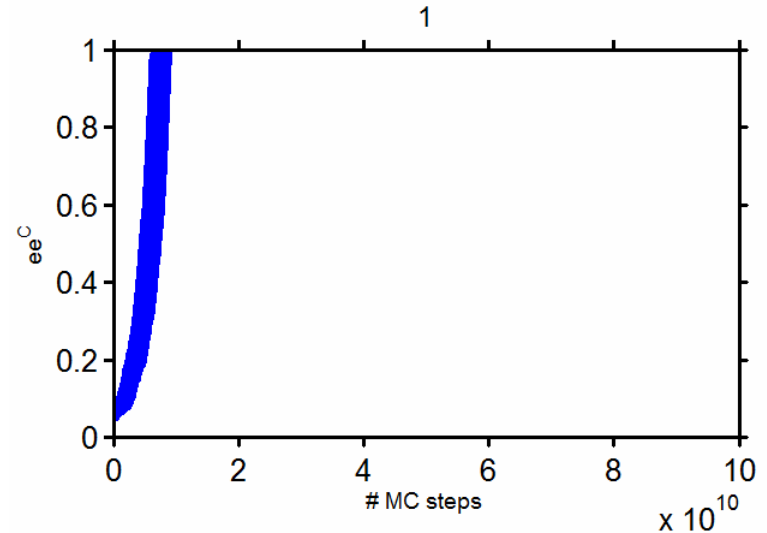
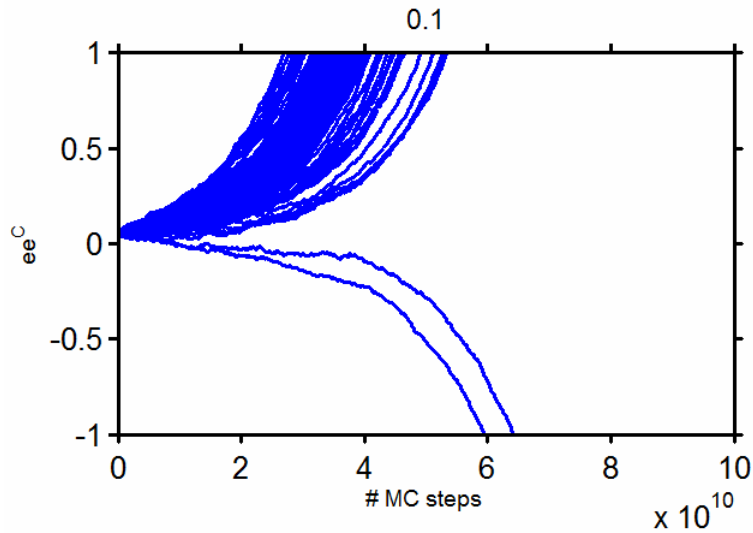
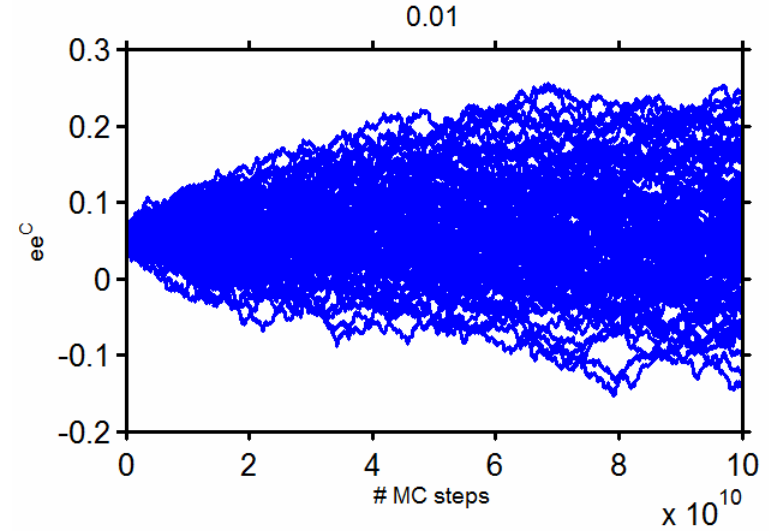
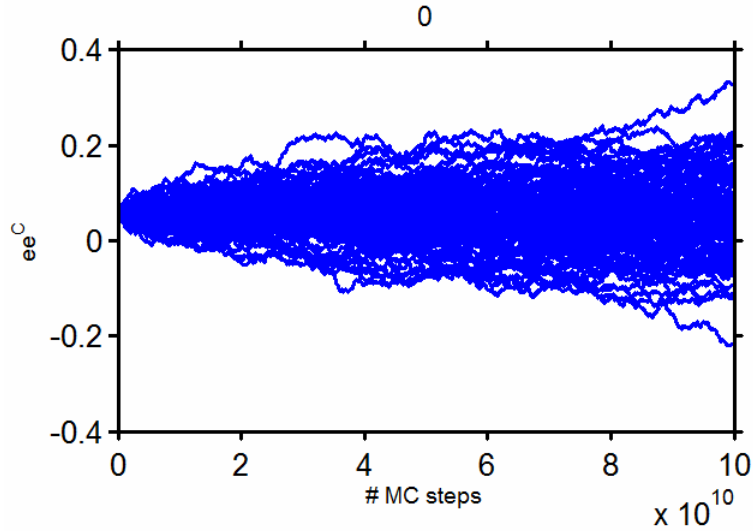
$$\beta E_{rac} = 5, p_{attr} = 0.4, K = 1, ee^C_0 = 0.055, N_{total} = 206660, N^{eq} = 10000, N^{L_0} = 10000$$



With agglomeration

$\beta E_{rac} = 5$, $p_{attr} = \text{varying}$, $K = 1$, $ee^C_0 = 0.055$, $N_{total} = 206660$, $N^{eq} = 10000$, $N^{L_0} = 10000$

ACS
 Presentation 4-
 9-13
 F.H. Stillinger
 View 21



With agglomeration

$\beta E_{rac} = 5$, $p_{attr} = \text{varying}$, $K = 1$, $ee^{C_0} = 0.055$, $N_{total} = 206660$, $N^{eq} = 10000$, $N^{L_0} = 10000$

